Fusion and compound nuclei decay for light and intermediate-mass systems: ^{24}Mg, $^{28}Si+^{12}C$, $^{24}Mg+^{24,26}Mg$, $^{28}Si+^{24}Mg$, $^{28,29,30}Si$

S. Gary* and C. Volant
Département de Physique Nucléaire, Centre d' Etudes Nucléaires de Saclay, 91191 Gif-sur-Yvette Cedex, France
(Received 27 July 1981)

Complete fusion or residue distributions have been measured with several experimental techniques for the following systems: ^{24}Mg, $^{28}Si+^{12}C$, $^{24}Mg+^{24,26}Mg$, $^{28}Si+^{24}Mg$, $^{28,29,30}Si$. The range of energies spreads from 1 to 3 times the Coulomb barrier. None of these systems presents structures in its fusion excitation function as pronounced as the ones observed for lighter entrance channels. The intensities of the residue distribution are generally in agreement with the predictions of a multiple deexcitation code. The shape and absolute values of complete fusion excitation functions are compared to macroscopic models and to the predictions of a coupled-channels approach of the reaction, which gives a more satisfactory account of experimental data.

NUCLEAR REACTIONS Fusion, measured $\sigma_{fusion}(E,\theta)$, $\sigma_{residue}(E,\theta)$; $^{24}Mg+^{12}C$, $16.4<E_{c.m.}<29.8$ MeV; $^{28}Si+^{12}C$, $15.1<E_{c.m.}<24.6$ MeV; $^{24}Mg+^{24}Mg$, $21<E_{c.m.}<41.6$ MeV; $^{24}Mg+^{26}Mg$, $20.3<E_{c.m.}<32.9$ MeV; $^{28}Si+^{24}Mg$, $24.2<E_{c.m.}<38.1$ MeV; $^{28}Si+^{28}Si$, $27.9<E_{c.m.}<41.4$ MeV; $^{28}Si+^{29}Si$, $27.4<E_{c.m.}<42.1$ MeV; $^{28}Si+^{30}Si$, $27.3<E_{c.m.}<42.8$ MeV; comparison with evaporation calculation; barrier parameters deduced from $\sigma_{CF}(E)$. Comparison of $\sigma_{CF}(E)$ with macroscopic models; coupled-channels approach of the fusion strength.

I. INTRODUCTION

The body of data now available in heavy ion fusion reactions has revealed at least two unexpected features in the excitation functions $\sigma_{CF}(E)$ (CF, complete fusion) relative to light- and medium-mass nuclei:

(i) Marked structures (up to 20% peak to valley ratio) were observed in the excitation function of $^{12}C+^{12}C$, ^{16}O and $^{16}O+^{16}O$ (Refs. 1–4) systems which all involve "α-particle-like" nuclei. Furthermore, the structures in $\sigma_{CF}(E)$ have been clearly correlated, at least for $^{12}C+^{12}C$, ^{16}O (Refs. 1 and 5) to the ones observed in the excitation functions of integrated inelastic scattering to the lowest lying excited states of the entrance channel nuclei.

(ii) The second point consisted of large unexplained differences between the cross sections $\sigma_{CF}(E)$ for entrance channels differing only by the neutron number of the targets; these differences have been observed either for high energy (^{15}N, $^{14}N+^{12}C$) (Ref. 1) or for Coulomb barrier energies (^{40}Ar, $^{16}O+^{148\rightarrow154}Sm$) (Refs. 6 and 7), ($^{35}Cl+^{58\rightarrow64}Ni$) (Ref. 8) and in this last case the influence of deformation has been put forward to explain at least part of the differences.

In order to investigate the first point, we chose to study entrance channels involving ^{24}Mg and ^{28}Si, which are the next candidates as nuclei whose mass and atomic numbers are a multiple of those of an α particle (^{20}Ne is not available as a beam on tandem accelerators).

The recent results of the Rochester group, showing strong structures in backward angles elastic and inelastic cross sections of ^{24}Mg, $^{28}Si+^{12}C$ (Refs. 9 and 10), prompted us to study the energy dependence $\sigma_{CF}(E)$ for these two systems. The investigation of the fusion behavior of $^{24}Mg+^{24}Mg$ and $^{28}Si+^{28}Si$ also corresponds to the search of oscillatory structures, which might be enhanced by the lack of odd partial waves due to the symmetry of entrance channels.

The availability of several isotopes of Mg and Si allowed us to extend our study to $^{28}Si+^{29,30}Si$ and $^{24}Mg+^{26}Mg$, thus probing the influence of neutron excess on the absolute value of σ_{CF} in the range of

energies we studied. Furthermore, one can expect interesting effects linked to the large deformation of ^{24}Mg and ^{28}Si. For the sake of completeness, we also investigated the fusion of ^{28}Si+^{24}Mg.

In the next section, we will present the experimental details relevant to each system. In Sec. III we will focus on the cross sections ($d\sigma/d\Omega$ or integrated cross section) of the elemental residues. The last section will be devoted to the "macroscopic" and "microscopic" aspects in the behavior of $\sigma_{CF}(E)$.

II. EXPERIMENTAL PROCEDURES AND DATA ANALYSIS

A. Beams and targets

The beams used in this series of experiments were produced with a gaseous (^{12}C, ^{28}Si) or a sputtering (^{24}Mg) source, and accelerated by the Saclay tandem Van de Graaff. The range of energy available is located near the Coulomb barrier E_B, up to about $1.5E_B$ for most of the intermediate mass systems, and slightly shifted to higher energies for ^{28}Si, ^{24}Mg+^{12}C.

A typical intensity for the ^{12}C, ^{28}Si beams was 50 nA, which was reduced at forward angles, but for the ^{24}Mg ions the intensity was not higher than 10 nA. The target thicknesses were chosen by making a compromise between reasonable counting rates and the available beam intensities. All the Si and Mg targets were deposited on C backing and their isotopical enrichment was better than 95%. The detailed characteristics of the targets and their backing, as well as the order of magnitude of the mean energy loss in the target, are given in Table I. All the targets also had a gold deposit (e_{Au} <5 μg/cm^2) for monitoring purposes.

B. Detectors

The fusion residues resulting from the deexcitation of the compound nucleus (CN) were detected directly, and identified either by their atomic num-

TABLE I. Characteristics of the targets used for these experiments. $\Delta E_{c.m.}$ is the loss of energy through the target averaged on the energy intervals given in Tables II–IV.

System	Target	Thickness of the C backing μg/cm^2	Target thickness μg/cm^2	Isotopical enrichment	$\Delta E_{c.m.}$ keV
^{24}Mg+^{12}C	^{12}C		40	natural	±85
	^{24}Mg	18	34	^{24}Mg: 99.94%	±30
^{28}Si+^{12}C	^{12}C		100	natural	±250
	^{12}C	80[a]	28	natural	±70
^{24}Mg+^{24}Mg	^{24}Mg	42	184	^{24}Mg: 99.94%	±450
^{24}Mg+^{26}Mg	^{26}Mg	42	156	^{26}Mg: 99.77%	±400
^{28}Si+^{24}Mg	^{24}Mg	28	80	^{24}Mg: 99.94%	±200
^{28}Si+^{28}Si	^{28}Si	20	30	^{28}Si: 99.91%	±100
^{28}Si+^{29}Si	^{29}Si	20	28	^{29}Si: 95% ^{28}Si: 4.7%	±100
^{28}Si+^{30}Si	^{30}Si	20	30	^{30}Si: 95.2% ^{28}Si: 4.18%	±100

[a] ^{24}Mg backing.

ber or by their mass. In the first case, we used a telescope ($\Delta E,E$), the ΔE measurement of which was made by a thin (3.3 μm) solid state detector (ΔE_S) or a gas-flow ionization chamber (ΔE_G), while the E detector was a conventional solid state detector whose thickness was chosen to stop all the heavy ions resulting from the reaction.

(a) The ΔE_S arrangement and reaction chamber have already been described in Ref. 1. It was used for the $^{24}Mg_P+^{12}C_T$, $^{24}Mg+^{24}Mg$ reactions (P, projectile; T, target) and allowed clear separation of the fusion residues from all other products.

(b) The ΔE_G detection system consisted of a classical, monoangular, gas-flow ionization chamber (90% Ar+10% CH_4) of the type described by Gamp *et al.*,[11] and the reaction chamber was the same one as for ΔE_S. The window of the ionization chamber ($\phi=2$ mm$\leftrightarrow\Delta\theta=\pm0.14°$) was made of Parylen-C (0.3 μm); the counter was operated at pressures varying between 10 and 30 Torr, depending on the mass and energy ranges of the residues to be detected, and the E detector was placed inside. This telescope was used to investigate $\sigma_{CF}(E)$ for $^{24}Mg_P+^{26}Mg_T$ and $^{12}C_P+^{24}Mg_T$, as well as for two measurements at fixed energies for $^{24}Mg_P+^{12}C_T$; in this last case the resolution of the detector enabled us to separate all the residues according to Z (Fig. 1). As already said in Ref. 1, the beam was tightly collimated at the entrance of the reaction chamber by two antiscattering slits (1×2 mm^2).

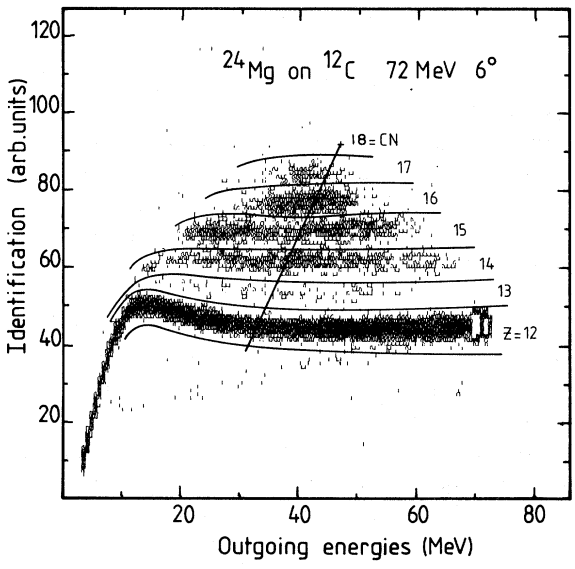

FIG. 1. Typical bidimensional spectrum *Id-E* obtained with an ionization chamber.

(c) The third experimental arrangement, a time of flight measurement (TOF), was set up to remedy the shortcomings of a ΔE-E type detection for the high masses and low energies encountered in the intermediate-mass systems. The kind of detection we have adopted allowed very low-energy (down to 5 MeV) residues to be detected and identified without significative loss of efficiency.

The ions passed through a thin C foil (8 μg/cm^2), placed at 35 cm of the target, and at 45° to the axis of the flight path; the secondary electrons produced at the surface of the foil were accelerated by a 1.45 kV voltage to the entrance of a channel electron multiplier [microchannel plates (MCP)]. The output of the MCP was collected by a conic anod and fed into a homemade constant fraction discriminator. The ions were stopped at the end of the flight path (70 cm) by a solid state detector (thickness $\simeq$50 μm), which was cooled down to 0°C, and overbiased by a factor of 2 in order to improve its time and energy resolutions; the corresponding preamplifier was installed in a vacuum in order to minimize the wire length.

The solid angle of detection was defined by a $\phi=4$ or 6 mm diaphragm, placed at the end of the flight path ($\Delta\theta=\pm0.11°$ or $\pm0.16°$), while the carbon foil of the start detector was collimated by a brass cylinder of 1 cm diameter. By taking a solid angle larger for the start than for the stop detector, one thus compensates for possible small angle scattering in the carbon foil.

The typical FWHM resolutions were $\delta E=150$ keV and $\delta t=160$ ps for 56 MeV ^{16}O ions. In the case of an 80 MeV ^{28}Si beam, the best results were $\delta E\simeq250$ keV and $\delta t\simeq250$ ps. A typical identification Et^2 ($\simeq A$) vs E spectrum is presented in Fig. 2 for the reaction $^{28}Si_P+^{29}Si_T$ at $E_{lab}=80$ MeV, $\theta_{lab}=6°$. Masses ranging from 31 to 38 are the fusion residues of ^{28}Si with the ^{12}C backing of the target, while masses 41 and 42 are the predominant decay channels of $^{28}Si_P+^{16}O_T$, ^{16}O being a contaminant of the Si target. One can see that the resolution allows individual separation of all the masses corresponding to the fusion residues relative to $^{28}Si_P+^{12}C_T$, $^{16}O_T$. The upper part of the bidimensional spectrum corresponds to the residual nuclei of $^{28}Si_P+^{29}Si_T$: The experimental resolution and the reaction dynamics allow one to separate groups of masses corresponding to (0α, x nucleons), (1α, y nucleons), and (2α, z nucleons) evaporated from the compound nucleus. The mass calibration was given by the heavy recoil peaks of ^{16}O scattering on ^{32}S and ^{56}Fe targets, and it con-

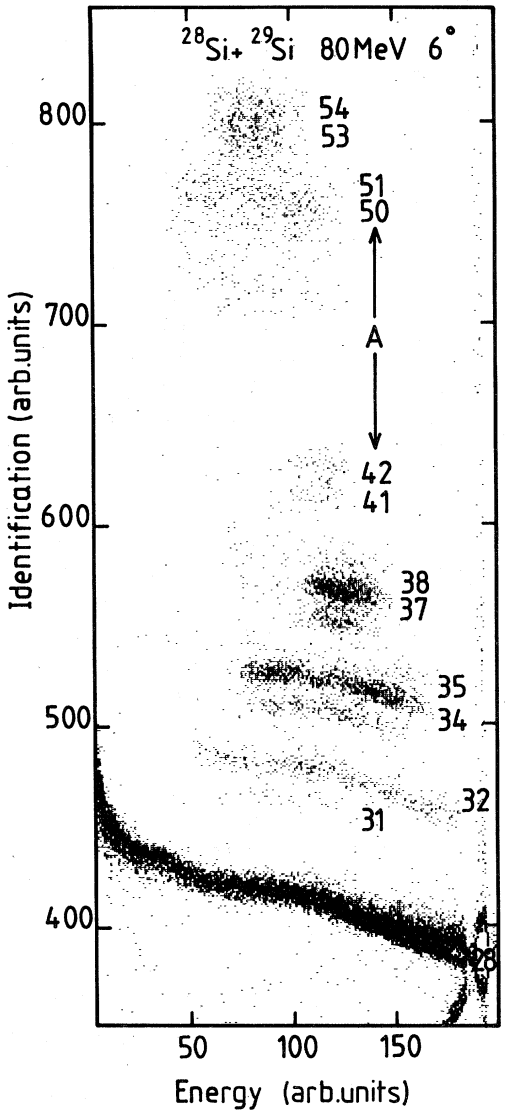

FIG. 2. Bidimensional plot *Id-E* obtained with a time of flight detection and corresponding to the residual nuclei of the reactions $^{28}Si_P+^{29}Si_T$, $^{16}O_T$, $^{12}C_T$ (from top to bottom).

firmed a linear mass scaling based on ^{16}O and ^{28}Si direct elastic scattering. When a full mass identification has been achieved (e.g., $^{28}Si+^{12}C$), it also helped us to establish the mass calibration.

Each event reaching the E detector was recorded on magnetic tape, together with the time of flight t and a computed identification proportional to Et^2. The events corresponding to a missing t signal (no signal coming from the MCP) have also been recorded in order to test the efficiency of the MCP detector, and to keep the ratio of $(E_{\text{alone}})/(E,t)$ events negligible. On the other hand, the geometrical efficiency between the two detectors "start" and "stop" is very close to one, because care was taken that the solid angle of the start be greater than the one spanned by the stop. This has been checked experimentally by measuring the angular distribution of elastically scattered heavy recoil of ^{16}O incident on an Fe target, at Coulomb and sub-Coulomb energies, where it follows Rutherford's law.

The TOF apparatus was mounted on a secondary arm, which moved around an axis located at the entrance of the beam in a 2 m-diameter chamber. The targets were also centered on this axis. Right and left elastic scattering measurements allowed determination of the effective zero degree. The size of the beam on the target was constrained to a 1×2 mm^2 spot by antiscattering polished cylinders placed before the entrance of the chamber ($\Delta\theta_{\text{beam}}\simeq0.02°$). The following systems were investigated with this TOF detection: $^{28}Si_P+^{12}C_T$, $^{24}Mg_T$, $^{28-30}Si_T$; in the last four systems the resolution enabled us to separate groups of masses [$\leftrightarrow0\alpha$, 1α, 2α emitted from the compound nucleus, which we will refer to as "0α emission" residues (or 1α, 2α)], while for $^{28}Si_P+^{12}C_T$ a complete mass identification was achieved (cf. Fig. 2).

For the three experimental setups, a monitor detector located at $\theta_{\text{lab}}\simeq20$, 25° was used for normalizing purposes.

C. Data analysis

For each system, the excitation function of total fusion (or of individual residues) integrated cross sections $\sigma_{\text{CF}}(E)$ were measured in two stages:

(a) First we investigated *complete angular distributions* ($d\sigma/d\theta$) at a few energies (usually four) evenly distributed along the excitation function. The range of measurements extended from 3°—4° to 30°, with an angular step usually varying between 1° at forward angles, and 5° at the back of the angular distributions, where $d\sigma/d\theta$ varies more smoothly. We also performed cross measurements to check the stability of the target.

At each energy we obtained simultaneously elastic scattering and fusion counts of the projectile P onto the target T, as well as elastic scattering counts of $P+$Au detected in the monitor detector. Arbitrary-unit values for fusion and elastic scattering cross sections were obtained relative to the monitor counts of $P+$Au elastic scattering. The

normalization of elastic scattering angular distributions $P+T$ to optical model predictions (which, for the highest mass systems or low angles reduce to Rutherford scattering) gave an absolute normalization for each energy, by means of which we obtained the absolute values for the angular distributions of fusion (residue) cross sections.

(b) In a second step, *excitation functions* were measured *at a fixed angle* θ_E^{lab} with a fine energy step (1 MeV $\lesssim \Delta E_{\text{lab}} \lesssim$ 2 MeV). The angle θ_E^{lab} was fixed to 5° or 6° and is reported for each system in Tables II–IV. Every five or six measurements, some points at fixed energies were remeasured in order to check the stability of the target. The absolute values $(d\sigma/d\theta)_{\text{CF}}(E)$ were obtained through the previously determined normalization of the angular distributions. Since the shape of $(d\sigma/d\theta)$ changes smoothly with energy, we linearly interpolated the experimentally measured ratios $R(E) = \sigma(E)/(d\sigma/d\theta)(E,\theta_E)$ obtained in the previous stage in order to convert at each energy angular differential cross sections $(d\sigma/d\theta)_{\text{CF(residue)}}$ into integrated cross sections $\sigma_{\text{CF(residue)}}$.

(c) The *relative uncertainties* within the fusion excitation functions are of the order of 4%; they arise from statistics ($N_{\text{CF}} \simeq 1000$, 2000 counts), interpolation of the ratio $R(E)$, and the more or less clear separation of fusion products. Except when stated otherwise, we did not take in account any error associated with the extrapolation of the measured angular distributions towards 0° or angles greater than 30°, because we feel the method used to reconstruct the whole of $(d\sigma/d\theta)$ is very reliable (see Sec. III). Angular distributions relative to elementary strength or complete fusion at low energy are affected by greater errors ($> 10\%$) because of much poorer statistics; moreover, the identification of very low populated residues ($\sigma < 20$ mb) might be contaminated by the tails of more populated residues of neighboring identification, and this can lead to errors far more important than 10%.

Other possible sources of error might occur while separating fusion residues as a whole:

(i) In the case of a $(\Delta E, E)$ detection, part of the very low energy spectra of fusion products can mix with other reaction products in the common Bragg curve (inelastic tail of the projectile identification, reaction with a target contaminant . . .); the following underestimation of the fusion counts might be estimated at less than 2%, by extrapolating the low energy spectrum, and one must stress that this error contributes only for the very low bombarding energies.

(ii) Contaminants of the target might lead to fusion residues whose identifications overlap with the principal fusion products. In the case of ^{29,30}Si targets, ^{28}Si was unavoidably present ($\simeq$4, 5%) in the enriched targets, and we subtracted the contribution of the $^{28}\text{Si}+^{28}\text{Si}$ reaction from each residue. In the case of $^{12}\text{C}_P+^{24}\text{Mg}_T$, contours delimiting fusion as a whole have been drawn in order to eliminate the contamination by the parasitic reaction $^{12}\text{C}_P+^{16}\text{O}_T$, and we believe no error was committed in the process.

For the $^{28}\text{Si}_P$, $^{24}\text{Mg}_P+^{12}\text{C}_T$ reactions, we were not able to detect fusion residues whose identification was the same (within $\pm$ one unit) as the projectile one; nevertheless, the error thus committed is negligible because the range of energies we have studied is not high enough to allow this kind of decay to occur with an intensity greater than 10 mb (for the highest excitation energy).

The *absolute normalization* of the excitation function has been determined with an *error* varying between ± 2 and $\pm 5\%$ according to the systems.

III. EXPERIMENTAL CHARACTERISTICS OF THE DEEXCITATION PROCESS

In this section we will analyze the characteristics of the residues that have been identified by means of one of the technical apparatus described above. Studies concerning the elementary redistribution of σ_{CF} are less numerous than those referring to total fusion. Yet, this aspect should not be neglected, because it can provide many details on the reaction mechanisms:

(i) Angular distributions of the residual nuclei are sensitive to the decay mode, since α emission gives more transverse momentum than nucleon emission. In some cases, a careful study of the shape of $(d\sigma/d\theta)$ can provide insights on the nature of the residual nuclei when a complete identification is not available experimentally.

(ii) The integrated cross sections σ_{res} (mb) might be compared to the predictions of a multiple deexcitation code such as CASCADE,[12] of which we made extensive use, in order to test the accuracy of the statistical treatment of the compound nucleus decay.

(iii) Another interesting feature resides in the study of excitation functions of each residue. In the range of energy we have explored, the high angular momenta J_{CN} decay primarily by emission of

TABLE II. Total fusion cross sections for $^{24}Mg+^{12}C$, $^{28}Si+^{12}C$, and $^{28}Si+^{24}Mg$. The underlined energies correspond to measurements of a full angular distribution, while at other energies, monoangular measurements were made at θ_E^{lab}, given at the bottom of the table. The quoted uncertainties are the relative errors while the normalization error is given by ϵ_{norm}.

$^{24}Mg+^{12}C$[a]				$^{28}Si+^{12}C$[b]		$^{28}Si+^{24}Mg$[c]	
$E_{c.m.}$ (MeV)	σ_{CF} (mb)	$E_{c.m.}$ (MeV)	σ_{CF} (mb)	$E_{c.m.}$ (MeV)	σ_{CF} (mb)	$E_{c.m.}$ (MeV)	σ_{CF} (mb)
16.37	*504±20*	24.83	1019±31	15.15	318±13	24.23	27.5±2
17.70	*604±25*	25.17	1049±31	*16.11*	*350±14*	25.15	66 ±3
19.03	*718±30*	25.50	992±30	16.26	386±15	25.15	60 ±4
19.70	*763±31*	25.83	993±30	16.26	415±17	26.08	113 ±3
20.37	*803±32*	26.17	1017±31	17.16	454±18	27	188 ±6
21.03	*859±35*	26.50	1032±31	18.06	548±22	27.69	238 ±7
21.03	*862±35*	27.17	1014±31	*18.24*	*538±22*	28.38	273 ±8
21.27	*846±35*	27.17	990±30	18.96	608±24	28.38	262 ±8
21.37	*873±35*	27.17	1035±31	20.76	672±27	29.31	344 ±10
21.70	*881±35*	*27.25*	*1040±42*	21.69	721±29	30.23	351 ±10
22.37	*890±36*	27.50	1041±31	*22.02*	*689±28*	31.15	428 ±13
22.70	*921±37*	27.83	1004±30	22.59	791±32	32.08	478 ±14
22.70	*880±35*	28.17	966±29	23.49	775±31	33	529 ±20
22.83	945±28	28.50	1002±30	24.39	879±35	34.15	604 ±18
23.17	947±28	28.83	999±30	*24.60*	*834±33*	34.85	582 ±23
23.50	1010±30	29.17	955±29	24.64	852±34	35.77	605 ±24
23.83	1027±31	29.5	1041±31			36.69	669 ±25
24.17	1047±31	29.83	1011±30			37.62	716 ±28
24.50	1024±31					38.08	762 ±23

[a]Italic: ^{24}Mg projectile; otherwise ^{12}C projectile; for both $\epsilon_{norm}=\pm5\%$, $\theta_E^{lab}=6°$.
[b]Italic: ($^{24}Mg+^{12}C$) target; $\epsilon_{norm}=\pm3\%$; otherwise ^{12}C target; $\epsilon_{norm}=\pm2\%$; $\theta_E^{lab}=5°$ for both measurements.
[c]$\epsilon_{norm}=\pm3\%$; $\theta_E^{lab}=5°$.

TABLE III. Total fusion cross sections for $^{24}Mg_P+^{24}Mg_T$, $^{26}Mg_T$; see Table II for a detailed caption. $\theta_E^{lab}=6°$ for both systems.

	$^{24}Mg+^{24}Mg$[a]			$^{24}Mg+^{26}Mg$[b]	
$E_{c.m.}$ (MeV)	σ_{CF} (mb)	$E_{c.m.}$ (MeV)	σ_{CF} (mb)	$E_{c.m.}$ (MeV)	σ_{CF} (mb)
21	25±2	32.05	729±36	20.32	28±2.5
22.5	85±4	32.05	745±30	21.89	120±5
22.5	80±5	33.05	784±25	21.89	110±5
24	184±9	34.06	790±25	23.46	241±5
25.5	303±15	34.8	901±27	25.03	363±8
27	388±16	36.08	870±27	26.59	468±11
28	492±21	36.82	956±36	28.16	574±29
28	538±20	37.6	935±33	28.16	559±13
29	568±26	38.6	961±48	29.73	661±16
29	585±30	39.6	1057±36	31.30	712±17
30	613±20	40.6	1031±33	32.87	820±24
31	627±27	41.60	1000±32	32.87	802±24
31	704±35				

[a] $\epsilon_{norm}=\pm 5\%$.
[b] $\epsilon_{norm}=\pm 3\%$.

α particles, while n,p emission is fed by the deexcitation of lower angular momenta; thus the corresponding residues are not sensitive to the same range of J_{CN}. For example, the oscillatory behavior of the $^{12}C+^{12}C$ fusion excitation function, which is correlated to perturbations of high angular momenta by the inelastic channels, is traced off in the excitation functions of α emission residues,

TABLE IV. Total fusion cross sections for $^{28}Si_P+^{28}Si_T$, $^{29}Si_T$, $^{30}Si_T$; see Table II for a detailed caption. $\theta_E^{lab}=5°$ for all systems.

	$^{28}Si+^{28}Si$[a]			$^{28}Si+^{29}Si$[b]		$^{28}Si+^{30}Si$[c]	
$E_{c.m.}$ (MeV)	σ_{CF} (mb)	$E_{c.m.}$ (MeV)	σ_{CF} (mb)	$E_{c.m.}$ (MeV)	σ_{CF} (mb)	$E_{c.m.}$ (MeV)	σ_{CF} (mb)
27.9	15±2	35.9	439±14	27.37	11.4±1.5	27.31	17±2
28.9	63±5	36.4	398±13	27.88	21.8±2.5	27.83	30±2
29.9	83±4	36.9	467±15	28.90	76±5	28.87	83±5
30.9	136±5	37.4	472±15	29.92	105±5	29.90	134±5
31.4	161±6	37.9	517±16	30.93	159±6	30.93	190±7
31.9	194±7	38.4	522±16	31.95	222±7	32.38	266±10
32.4	236±9	38.9	531±16	32.41	265±10	33	310±11
32.9	238±9	39.4	563±17	34.00	346±10	34.04	377±13
33.4	302±10	39.9	582±18	35.	400±12	35.07	445±14
33.9	304±9	40.9	689±21	36.02	522±16	36.11	469±15
34.9	369±12	41.4	615±22	36.89	554±10	36.88	548±16
35.4	372±12			38.06	560±12	37.66	526±17
				39.07	549±19	38.69	594±18
				40.09	609±21	39.73	665±20
				40.91	720±24	40.92	654±20
				42.13	722±26	41.80	765±27
						42.83	822±27

[a] $\epsilon_{norm}=\pm 5\%$.
[b] $\epsilon_{norm}=\pm 3\%$.
[c] $\epsilon_{norm}=\pm 2\%$.

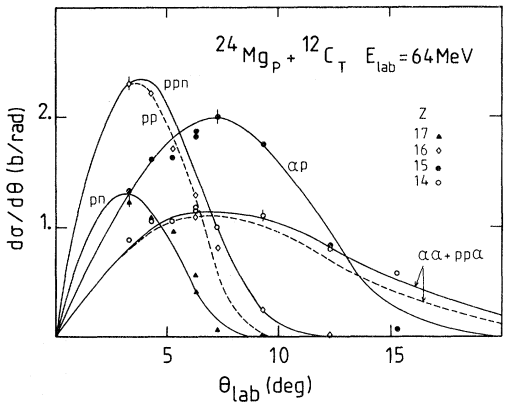

FIG. 3. Laboratory angular distributions of Z-separated fusion residues for the $^{24}Mg_P + ^{12}C_T$ system. The full and dashed curves correspond to theoretical predictions relative to the given sequences of evaporation (see text).

but not in those of nucleon emission products. Thus the study of excitation functions for individual residues can corroborate oscillations seen in $\sigma_{CF}(E)$, and by the same way give a hint on the process responsible for these possible structures.

The two first points will be discussed in this section, and the excitation functions will be presented in Sec. IV.

A. Angular distributions of fusion residues

The strong focusing towards zero degree of the residual nuclei angular distributions is one of the experimental difficulties which have to be solved in such studies. This problem is illustrated in Fig. 3 for the $^{24}Mg_P + ^{12}C_T$ system, which in this respect is one of the most difficult cases. The integration over angles of the residual nuclei cross section requires an extrapolation towards zero degree which, at least for the highest Z residues, is quite hazardous. The method we used consists of a careful analysis of the experimental angular distributions (and sometimes of the energy spectra) by a Monte Carlo code RECOIL2 which calculates the kinematics of the deexcitation. This program is described extensively in Refs. 13 and 14 and we will just remind you of its main features. The input consists of: (i) a given sequence of evaporation (xn, yp, $z\alpha$), (ii) the anisotropies of the angular distributions relative to the light particles (n, p, α), as well as (iii) the center-of-mass (c.m.) energy spectra of these particles.

The nucleon emission was supposed isotropic ($d\sigma/d\Omega$=constant), while the α emission is more focused ($d\sigma/d\Omega$=constant for $\theta<\theta_c$, $d\sigma/d\Omega \propto 1/\sin\theta$ for $\theta>\theta_c$). The parameter θ_c varied between 15° and 35° depending on systems and energies, and its value was fixed by fitting the experimental part of $(d\sigma/d\theta)_{res}$.

The center-of-mass energy spectra of n, p, α were taken from the multiple particle decay code CASCADE. The calculation was first run with the total fusion σ_{CF} as input [σ_{CF} was evaluated by rough integration of $(d\sigma/d\theta)^{exp}_{CF}$], and it gave integrated cross sections for each residue, σ_{res} (mb), as well as the energy spectra of the first emitted n, p, α particles. In order to take into account the shrinking of the excitation energy range with multiple emission, the c.m. spectra were compressed after each evaporation.[14]

The residue identification obtained experimentally allowed only A separation at best, and does not determine the sequence of evaporation; so, in chosing it as input for the RECOIL2 calculation, we had to rely on the results of the CASCADE calculation. These results show that in the mass and excitation-energy ranges of this study, the experimental identification nearly always corresponds to one predominant channel, which we then adopted to reproduce the whole of the angular distribution $(d\sigma/d\theta)_{res}$. When such a correspondence (identification $\leftrightarrow$ main sequence) was established, we found that the shape of the back part of $d\sigma/d\theta$ ($\theta>4°$, 5°) was very well reproduced by the RECOIL2 calculation. We then adopted the theoretical shape of $d\sigma/d\theta$ between 3°−4° and 0° to integrate accurately the experimental curve, while the integration at back angles relied on experimental points. In this way we think that one can get rid of the uncertainties attached to the extrapolation of $d\sigma/d\theta$ towards 0°.

To illustrate these calculations and emphasize what they can bring to the knowledge of the deexcitation process, we will discuss in detail Fig. 3, which shows the angular distributions of $^{24}Mg_P + ^{12}C_T$ heavy residues.

The relative features of nucleons/alpha evaporation residues are clearly seen:

(i) Residues of nucleon emission ($Z=17$, 16) are so strongly focused to forward angles that we did not succeed ($Z=17$) in detecting the maximum of $d\sigma/d\theta$. From this $Z=17$ example one can see the improvement brought by adopting a theoretically predicted shape for $d\sigma/d\theta$, rather than a linear extrapolation to 0°.

(ii) On the contrary, the experimental angular distributions of $Z=15$ and 14 exhibit well determined maxima and do not rely on extra calculations to be integrated.

The different curves and their labels (x nucleons, y alpha) have been determined according to CASCADE and RECOIL2. Q value conditions are such that both ^{30}Si ($\leftrightarrow pp\alpha$ emission) and ^{28}Si ($\leftrightarrow\alpha\alpha$) can contribute to the $Z=14$ strength; the experimental $(d\sigma/d\theta)_{Z=14}$ is broader than the one (dashed curve) predicted by the calculation when using the CASCADE isotopic ratio ($pp\alpha=40\%$, $\alpha\alpha=60\%$); a larger proportion of two alpha decay ($\alpha\alpha=80\%$) is in much better agreement with the back of the experimental $d\sigma/d\theta$ curve. This "guessed" percentage was later confirmed by a time of flight measurement, which gave the ratio $A=30$: 22%, $A=29$: 78%, and also proved the adequacy of the RECOIL2 $pp\alpha$ and $\alpha\alpha$ theoretical angular distributions. A careful analysis of the angular distributions thus appears to be a possibility to supply to the experimental identification.

This procedure was generalized in order to extrapolate the angular distributions found experimentally for each residue and for the total fusion towards zero degree and, thus, to integrate them with minimal errors. As an example, Figs. 4 and 5 sum up the angular distributions obtained for ^{28}Si+^{12}C and ^{28}Si+^{28}Si deexcitation products, as well as the curves adopted for their integration.

B. Integrated cross sections of residues: Comparison with the CASCADE predictions

The cross sections obtained by integration of the angular distributions relative to each residue (identified by Z, A or the number of α particles emitted from CN), have been compared to the predictions of the CASCADE deexcitation program.[12] This program has been successfully used to describe the deexcitation of several compound nuclei ($A_{CN}<60$) and thus it is well suited for the mass and excitation energy region we explored. Two sets of parameters were determined by Pühlhofer in order to best fit the relative weights of residues formed by deexcitation of various nuclei. The first one, which we labeled $LD1$, is taken from the study of light CN,[12] while the $LD2$ set refers to heavier CN ($A_{CN}\simeq 60$).[15] We considered each of these parametrizations as a whole, and we did not try to vary one specific parameter relative to a given nucleus (apart from the introduction of low-lying levels of the residual nuclei belonging to the decay chains).

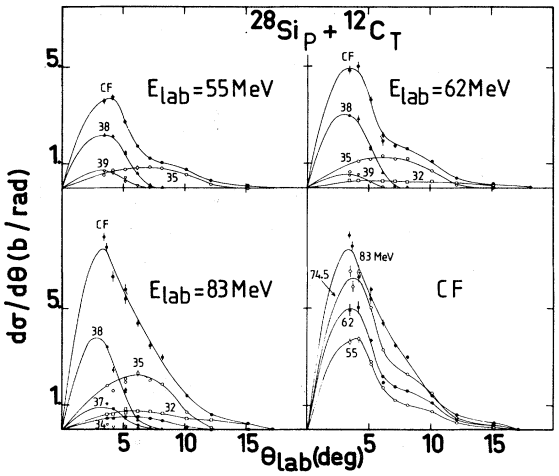

FIG. 4. Laboratory angular distributions of CF and mass-separated fusion residues for the $^{28}Si_P+^{12}C_T$ reaction at various incident energies. The curves are those adopted to integrate the angular distribution $d\sigma/d\theta$.

A comparison of the results obtained with these two parametrizations is presented in Fig. 6 for the medium-mass compound nucleus ^{40}Ca($\leftrightarrow^{28}$Si $+^{12}$C). The differences between the two theoretical predictions are noticeable only at high energy, and the most important ones, in relative values, occur for low-populated $A=34$ and 37 nuclei, the best agreement for these two residues being obtained with the $LD2$ family. On the whole, the agreement is fairly good. Nevertheless, one can notice systematic discrepancies which clearly exceed the range of a change relative to the

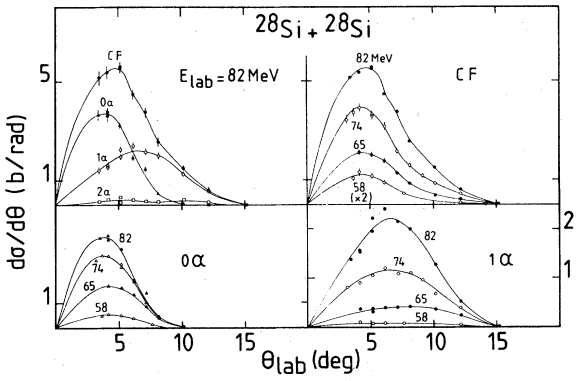

FIG. 5. Angular distributions of CF and "α emission" residues relative to the fusion of ^{28}Si+^{28}Si at various incident energies. The curves drawn through the experimental points are those adopted to integrate $d\sigma/d\theta$.

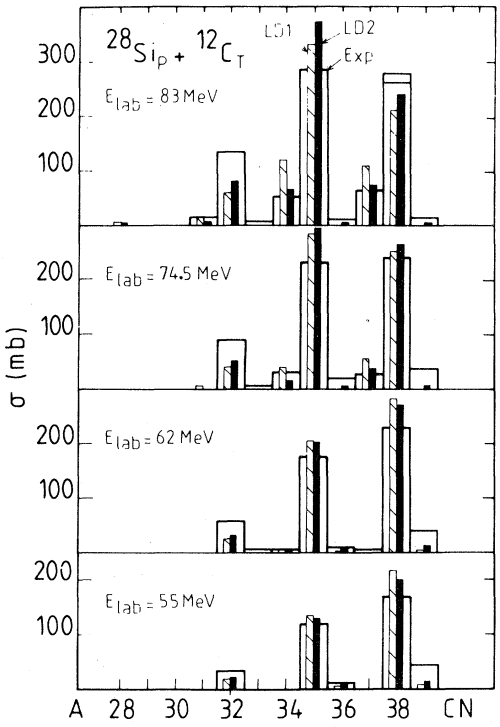

FIG. 6. Mass distribution of the $^{28}Si+^{12}C$ fusion residues at various incident energies compared to CASCADE predictions *LD*1 and *LD*2. The two experimental histograms for $A=38$, $E_{lab}=83$ MeV correspond to different extrapolations of $(d\sigma/d\theta)$ towards 0°, relative to these particular mass and energy.

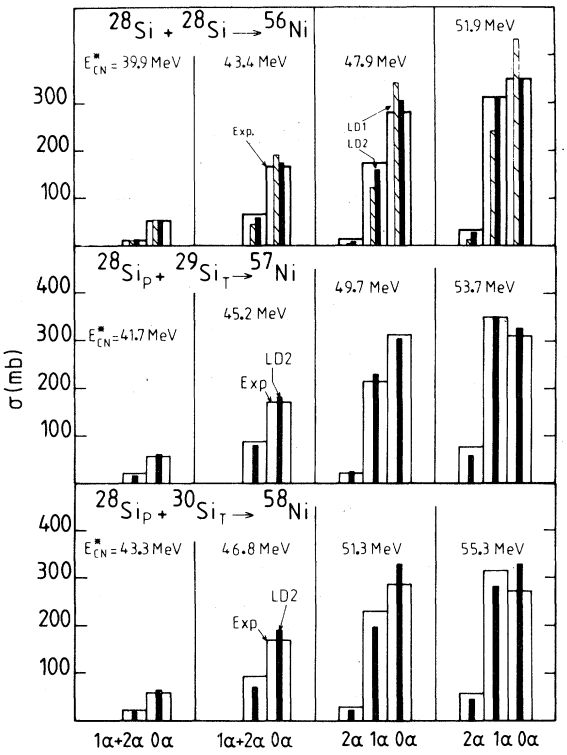

FIG. 7. Distributions of "α emission" residues relative to the fusion of the $^{28}Si_P+^{28-30}Si_T$ systems at various energies compared to the CASCADE theoretical results (*LD*1, *LD*2).

parametrization as a whole, and bear physical significance:

(i) The first is a considerable underestimation of σ ($A=39 \leftrightarrow$CN-1p); in fact it is indeed very odd that the compound nucleus deexcitation stops after emission of only one particle and, up to now, no other similar case can be found in the literature for a comparable excitation energy range ($E^* \simeq 30$ MeV).

(ii) Second, the 2α emission (CN$\rightarrow A=32$) is much underestimated (this is also true, though in a lesser extent, for $^{24}Mg+^{12}C$). This characteristic, often reported for relatively light ions, might be linked to the enhancement of α emission for high angular momenta due to the stretching of nuclei at high J, which implies a lower barrier energy.

In Fig. 7 we present the results obtained for the higher-mass systems $^{28}Si+^{28-30}Si$, which were studied at the same c.m. energies. The theoretical results are gathered according to the number of α particles emitted from each compound nucleus. The *LD*2 parametrization is, without surprise, more adequate to describe the ^{56}Ni deexcitation, which is indeed very well reproduced. The agreement for the other systems is satisfactory, though one notices a theoretical tendency to underestimate α emission as the target mass increases.

We have reported for each of these three systems (Fig. 8) the experimental ratios $(\sigma_{i\alpha}/\sigma_{CF})$ vs CN excitation energy, and one can notice a clear similarity of the decay chains relative to the three Ni isotopes. This behavior is not really surprising, since the angular momenta involved are about the same. Nevertheless, it is much more simple than the CASCADE predictions.

IV. EXCITATION FUNCTIONS

We will first present the excitation functions of all the systems studied and then discuss the qualitative and quantitative features of $\sigma_{CF}(E)$. For all the figures of subsection A we have adopted the following rule: Open dots correspond to complete angular distributions while full symbols refer to monoangular measurements at θ_E. Tables II–IV sum up all the total fusion cross sections for the

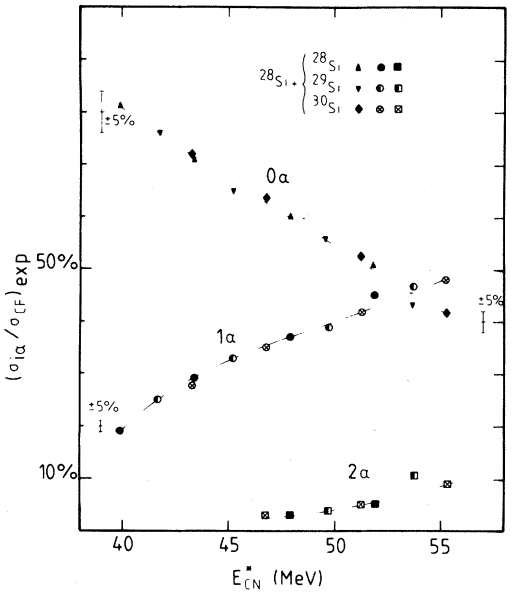

FIG. 8. Ratio of "α emission" residues to total fusion vs E^*_{CN} for the three systems ^{28}Si+$^{28-30}$Si. The curves are drawn to guide the eye.

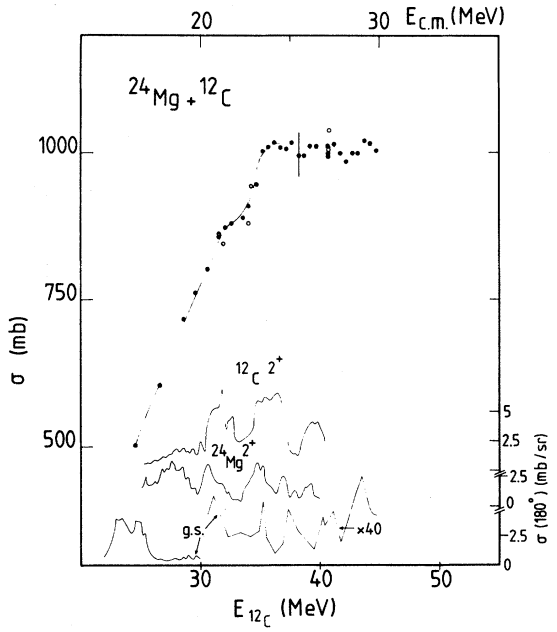

FIG. 9. Fusion excitation function for the ^{24}Mg+^{12}C system, the line drawn through the experimental points is only a guide to the eye. The curves at the bottom of the figure are the experimental excitation functions (Refs. 9 and 16) relative to back-angle scattering to the ground state and first inelastic states of the entrance channel.

various systems we studied and a detailed caption is given in Table II.

A. Experimental data

1. $^{24}Mg+^{12}C$

The results concerning $\sigma_{CF}(E)$ are reported in Fig. 9. The low energy part was performed with a ^{24}Mg beam and the detection was done with the previously described ΔE_S arrangement, while the highest energies were investigated with a ^{12}C projectile and a ΔE_G detector. The kinematics of the reaction or the Z resolution of the ΔE_S detector were such that Z separation was achieved only at two energies ($E_{^{24}MG}=64$, 82 MeV), and not all along the excitation function. Our experimental results show that σ_{CF} increases up to $E_{c.m.}\simeq 24$ MeV energy, from which it stays more or less constant ($\sigma_{CF}\simeq 1000$ mb). From this energy the excitation function presents very small structures ($\pm 3\%$) which, however, are of the magnitude of relative errors. These small accidents are not correlated in any obvious way either with the one of the backward quasielastic excitation functions,[9,16] or with the recently measured excitation function of the inelastic channel, integrated over angles (see Fig. 15); the excitation function $\sigma_{in}(E)$ of the 1.37 MeV channel does present some slight oscillatory structure, but the amplitude of these accidents (5 to 7 mb) does not seem strong enough to generate spectacular structures such as the ones observed for the ^{12}C+^{12}C system. The lowest energy cross sections of the excitation function might in fact be higher than measured due to the uncertainty of the extrapolation of the $d\sigma/d\theta$ shape obtained at $E_{^{24}Mg}=64$ MeV to such energies.

2. $^{28}Si_P+^{12}C_T$

Figure 10 shows the results obtained for CF and masses 38, 35, and 32 ($\leftrightarrow$ nucleons, 1α, 2α emission) which are the predominant residues. Our measurements were made on a pure C target (circles), and as a parasitic measurement of the $^{28}Si_P+^{24}Mg_T$ reaction, onto the C backing of the Mg target (squares). The two independent sets of data are in good agreement. No structures occur in the range of energy we have studied, neither for CF, nor for any of the residues, which should have presented more sensitivity to a possible accident relative to the total fusion, and yet, the range of energy we explored overlaps with the one in which

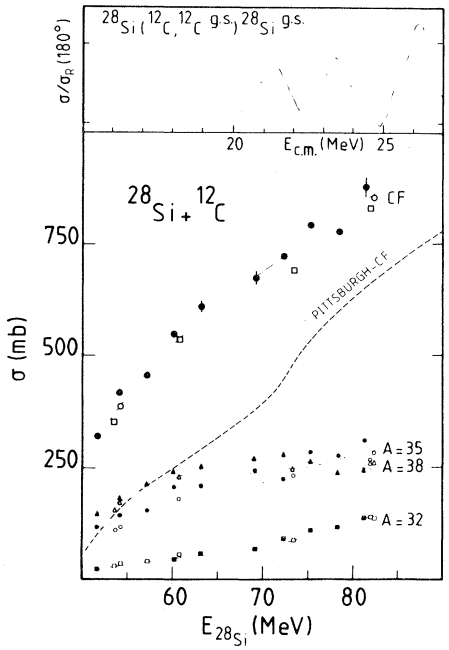

FIG. 10. Fusion excitation functions for the $^{28}Si+^{12}C$ systems; points refer to this work (see text) and the curve is only a guide to the eye, the dashed line is taken from Ref. 17. At the bottom of the figure are also shown the excitation functions for the principal residues of deexcitation ($A=38$, 35, and 32). The curve in the top inset represents back-angle elastic scattering measurements. (Reference 10.)

strong accidents were observed in the excitation function of quasielastic diffusion at 180°.[10] (Figure 10.)

Up to now, structures of the CF excitation function have always been linked to the ones observed in inelastic integrated excitation function; but we believe (i) that the observation of structures in a $d\sigma/d\Omega$ (180°) excitation function is not a sure sign of a more general "resonant" behavior concerning integrated cross sections of quasielastic channels; (ii) the inelastic channels, even if they do present accidents of $\sigma_{\text{int}}(E)$, are not important enough to reflect their structures onto $\sigma_{\text{CF}}(E)$, in contrast to the $^{12}C+^{12}C$, ^{16}O cases.

Figure 10 also reports CF measurements made at Pittsburgh[17]; the two sets of data completely disagree. We feel all the more confident in our data as we made two entirely independent series of measurements (circles and squares) and as preliminary data obtained at Seattle[18] (with a ^{28}Si beam and an ionization chamber) give cross sections in better agreement with our data. We suggest that

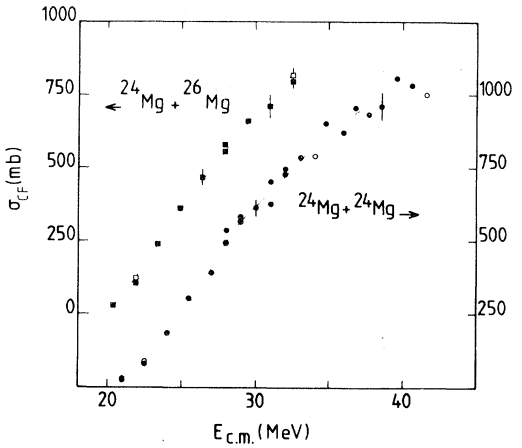

FIG. 11. Total fusion excitation function relative to $^{24}Mg+^{24}Mg$ and $^{24}Mg+^{26}Mg$ (the curves are drawn only to guide the eye).

the Pittsburgh measurements, obtained with a ^{12}C beam, could be underestimated owing to the difficulty of detecting very low energy heavy residues.

3. $^{24}Mg_P+^{24,26}Mg_T$

The fusion excitation functions of these two systems were measured with a ΔE_S ($^{24}Mg+^{24}Mg$) or a ΔE_G ($^{24}Mg+^{26}Mg$) detector (Fig. 11). The variation of σ_{CF} is quite smooth for the two systems. The behavior of the $^{24}Mg+^{24}Mg$ data at high energy is rather irregular, although the suggested "structures" are within the relative error bars.

4. $^{28}Si_P+^{24}Mg_T$, $^{28,29,30}Si_T$

The excitation functions of these various systems were investigated with the TOF apparatus allowing a separation of the residues according to the number of α particles emitted from CN. There are no evident structures in those excitation functions, either for CF or for any of the residues, except maybe in the high-energy part of $\sigma_{\text{CF}}(E)$ relative to $^{28}Si+^{28}Si$, which seems to present slight oscillations (see Fig. 12); nevertheless, the amplitude of these possible structures ($\pm 7\%$) is just a little greater than the error bars, and it is not possible to connect them either with 0α or 1α emission. The squares at $E_{\text{lab}}=80$ and 90 MeV represent measurements of Ref. 19; the discrepancy between the two data at 80 MeV reach 17%, but we do not

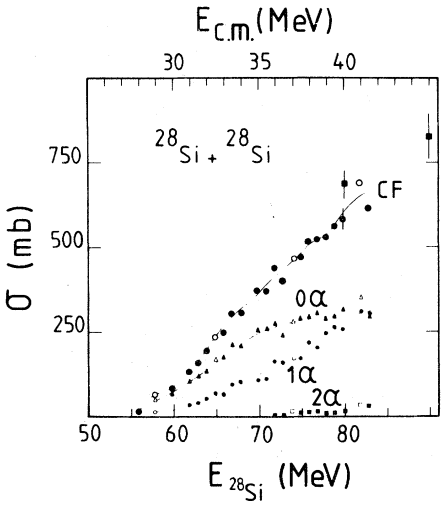

FIG. 12. Excitation function of total fusion and "α emission" residues for the ^{28}Si+^{28}Si system (the curves are a guide to the eye). We have also added two points (■) relative to complete fusion taken from Ref. 19.

have any other point of comparison available and we do not know if the disagreement concerns only one point or the absolute normalization. On the other hand, the comparison of the strengths for the various (comparable) residues are in good agreement for the two sets of data.

B. Discussion

The energy region of this work is always dominated by the barrier influence; apart from the cases of ^{24}Mg+^{12}C and perhaps ^{24}Mg+^{24}Mg, the maximum energy experimentally available did not allow us to study the region where the ratio σ_{CF}/σ_R drops sharply.

1. "Barrier parameters"

We first reduced our experimental data, relative to a given system to the most commonly used (V_B,R_B) parameters through the formula

$$\sigma_{CF}(E)=\pi R_B^2\left[1-\frac{V_B}{E_{c.m.}}\right]. \quad (1)$$

Table V gives the numerical values for each system, the error being of the order of ±5% for both parameters. A comparison of these (V_B,R_B) values with the systematic established by Kovar *et al.*[20] shows that the values relative to the intermediate-mass systems (^{24}Mg+^{24,26}Mg; ^{28}Si+^{24}Mg, $^{28-30}$Si) are in good agreement with the mean behavior observed for other medium-mass systems.

On the contrary, R_B (^{28}Si+^{12}C) and especially V_B (^{24}Mg+^{12}C) are very far from the "mean" values suggested by the trend of other light systems, a fact that confirms the peculiarity of the systems leading to compound nuclei of mass between 32 and 42.

2. Horn-Ferguson parametrization

An approach to fusion excitation functions similar to Eq. (1) but taking into account part of the energy dependence of the fusion barrier has been developed by Horn and Ferguson.[21] In their parametrization one writes

$$\sigma_{CF}(E)=\pi\rho^2\left[1-\frac{D}{\rho}\right], \quad (2)$$

where

TABLE V. Fusion barrier parameters V_B, R_B, r_B giving best fits to experimental fusion cross sections through Eq. (1). The error on both parameters is of the order of ±5%.

System	^{24}Mg+^{12}C	^{28}Si+^{12}C	^{24}Mg+^{24}Mg	^{24}Mg+^{26}Mg	^{28}Si+^{24}Mg	^{28}Si+^{28}Si	^{28}Si+^{29}Si	^{28}Si+^{30}Si
R_B (fm)	7.968	7.424	8.373	8.326	8.112	8.247	8.473	8.474
r_B (fm) = $R_B/(A_1^{1/3}+A_2^{1/3})$	1.54	1.394	1.451	1.424	1.37	1.358	1.387	1.38
V_B (MeV)	12.23	12.59	21.53	20.80	24.64	28.95	28.59	28.28

$$D=\frac{Z_P Z_T e^2}{E_{\text{c.m.}}} \text{ and } \rho=mE_{\text{c.m.}}+b \ .$$

The analysis of experimental data has enabled the authors to conclude that b was related to the charge-density radii of the incident nuclei, while m was suggested to depend on the mass of the compound system.

Lozano and Madurga[22] found that they could reproduce the fusion of many more systems by considering nuclear-density instead of charge-density distributions. b was thus considered as the sum of radii where the mass distributions fall to 0.002 nucleons/fm^3 and the corresponding formula for m was $m^{-1}=21\ (2.44-A_{\text{CN}}{}^{1/3})$ MeV/fm. We calculated $\sigma_{\text{CF}}(E)$ with the parametrization of Refs. 22 and 23; the theoretical values are compared to experimental data in Fig. 13. At very low energy ($E_{\text{c.m.}}\simeq E_B$), the comparison between experiment and theory is not any more relevant because the approximations leading to Eqs. (1) and (2) are not valid.

mass systems, the agreement is all the more satisfactory as there is no adjustable parameter. One should nevertheless notice that for intermediate mass systems involving ^{28}Si, there is a slight overestimate of σ_{CF}, while the agreement is remarkable for ^{24}Mg+^{24,26}Mg. On the contrary, the theoretical values obtained for ^{24}Mg, ^{28}Si+^{12}C overestimate the experimental data by as much as

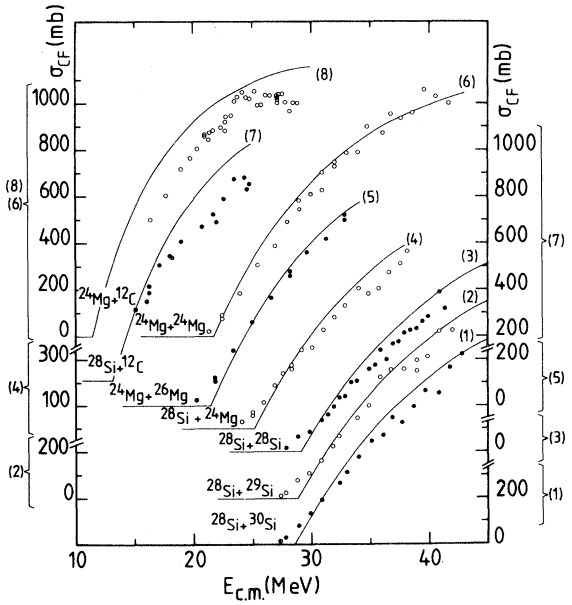

FIG. 13. Experimental (points) total fusion excitation functions compared to the predictions (lines) of Ref. 21 model, with a parametrization due to Refs. 22 and 23, for all the systems studied in this work.

100, 150 mb. In the range $22<E_{\text{c.m.}}<32$ MeV ^{24}Mg+^{24}Mg excitation function has a peculiar behavior: σ_{exp} is always less than σ_{th}, while for the neighboring ^{24}Mg+^{26}Mg the values agree.

3. *Bass potential*

We compared our experimental points to the theoretical predictions of this universal potential, because we feel that the comparison with a systematic behavior enables one to test the influence of the entrance channel particularities. This ion-ion potential has been deduced[24] from experimentally determined fusion cross sections, and particular care was taken by Bass to find a universal parametrization that reproduces a majority of fusion excitation functions without any parameter adjustment. The nuclear potential is defined by

(i) its depth

$$V_N(s)=\frac{R_1R_2}{R_1+R_2}g(s) \ ,$$

where

$$s=r-R_1-R_2$$

and

$$g(s)=\left[0.03\exp\frac{s}{3.3}+0.061\exp\frac{s}{0.65}\right]^{-1}$$

and (ii) radii

$$R_i=1.16A_i{}^{1/3}-1.39A_i{}^{-1/3} \ . \qquad (3)$$

The constants defining this radius R_i have been adjusted in order to obtain a best fit over a systematic of masses and systems, but nothing in the Bass approach forbids one to vary it slightly; such a procedure would only reflect the inability of a simple analytic formula to take into account all the deviations from a universal behavior of R_i. The theoretical predictions, corresponding to a value of radii given by Eq. (3), are reported as continuous lines on Fig. 14.

In the high energy part, the agreement is rather fair for systems involving ^{24}Mg; on the contrary, the fusion strength for systems involving ^{28}Si is generally overestimated. In order to get a better fit at high energy we diminished the radii characterizing the potential by 2% (dashed line) for all the ^{28}Si systems but ^{28}Si+^{28}Si, where the reduction reached 5%, a fact that suggests that the ^{28}Si fusion radius is much lower than the one given by Eq. (3).

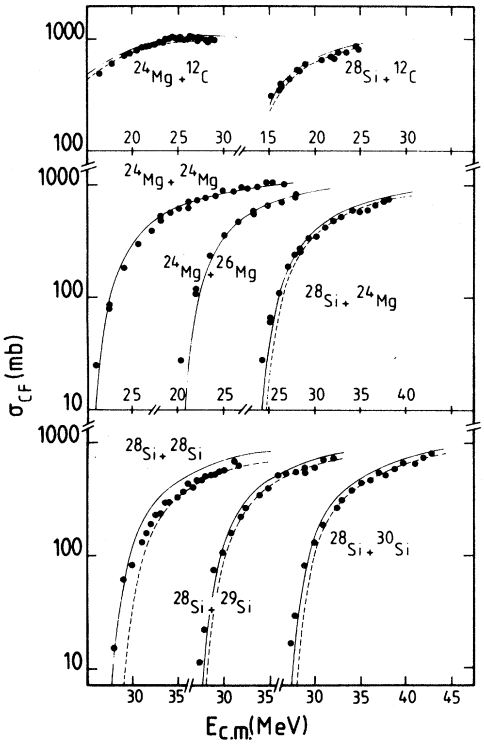

FIG. 14. Experimental fusion cross sections compared to Bass model predictions; full lines refer to a radius given by Eq. (3) while the dashed line corresponds to radii lowered in order to give a better fit of the high-energy part (see text).

One should notice the relative behavior of theoretical predictions (that best fit the high energy part) and experimental data at low energy where σ_{CF} is less than 100—200 mb. Except for the $^{24}Mg+^{24}Mg$ system, theory always underestimates the absolute value of σ_{CF} by a factor that increases with diminishing energy. This might be due to the influence of the high static deformation of entrance-channel nuclei which contributes to lower the Coulomb barrier and thus increases σ_{CF}.[8,6] In this respect, the behavior of $^{24}Mg+^{24}Mg$ is once more peculiar: Theory is in good agreement with experiment in a region where neighboring $^{24}Mg+^{26}Mg$ presents the usual underestimation, common to all the intermediate-mass systems we have studied.

4. *Coupled-channels calculations*

The Bass universal potential can reproduce in a satisfactory fashion the high-energy part of $\sigma_{CF}(E)$ for the systems we have studied; nevertheless, in order to obtain such an agreement we had to slightly reduce the radii parametrizing the potential, and it was impossible to give an account of the fusion strength for $\sigma_{CF} < 100-200$ mb, the observed discrepancy originating, according to us, from the large deformations of the incident ions. This suggests that one must take into account the particularities of the entrance channels in order to give a good estimate of the fusion cross section over a range of energy and systems as large as possible.

We have thus undertaken an analysis of the reaction flux within the coupled-channels model. The calculations we made are certainly perfectible, because in the course of this analysis we were faced with a nearly complete lack of experimental data concerning the integrated strengths towards the first inelastic states, data which could have enabled us to ascertain the validity of our optical model parametrization. Inelastic angular distributions, which are analyzed in the literature in order to obtain parameters describing the scattering of the two incident ions, are not adequate experimental data for accurate determination of σ_{in} since the part of the angular distribution located at forward angles, where no experimental points are available, is not at all negligible to evaluate the integrated inelastic cross section.

Such an approach has already been followed by Stokstad *et al.*[35] for higher mass systems. Owing to the low (sub-Coulomb) energy range studied, inelastic scattering cross sections were much more dependent on the approximation made to calculate this inelastic contribution than in the mass and energy range we deal with.

In our case, it seems to us that a coupled-channels approach should give a reasonable account of the fusion cross sections if one uses parameters taken from the literature which roughly give the amplitude of the inelastic cross sections. The studied energy range is high enough above the Coulomb barrier so that the theoretical uncertainties on the inelastic cross sections do not affect very much the fusion cross section which in this approach is given by $\sigma_{CF}=\sigma_R-\sigma_{in}$.

Procedure

(i) Both nuclei of the entrance channels we have studied have static deformations; the code ECIS (Ref. 25) we used allows deformation and excitation to inelastic states of only one nucleus. We thus performed two separate calculations: The first one allows excitation of one of the entrance

channel nuclei, and, in a second part, we proceeded to deform and excite the other nucleus (but we kept the same optical parametrization).

(ii) The optical part parameters, as well as the deformations, were taken from the literature, where they usually are the results of best fit searches relative to elastic and (first) inelastic scattering angular distributions of the system itself or of a neighboring one. Table VI sums up the parametrizations used in the course of these calculations as well as the references where they were given.

Let us briefly and precisely define the various parameters; the nuclear part of the potential is conventionally given by a Woods-Saxon real and imaginary form factor

$$V_{\mathrm{re}}(r)=-\frac{V}{1+\exp\frac{r-R_V}{a_V}},$$

$$W_{\mathrm{im}}(r)=-\frac{W}{1+\exp\frac{r-R_W}{a_W}}$$

and the Coulomb part is defined by

$$V_C(r)=\frac{Z_P Z_T e^2}{r} \quad \text{for } r>R_C\ ,$$

$$V_C(r)=\frac{Z_P Z_T e^2}{2R_C}\left[3-\frac{r^2}{{R_C}^2}\right] \quad \text{for } r<R_C\ .$$

The angular dependence of the potential radii R_V, R_W is given by

$$R_V(\theta)=r_0^V({A_P}^{1/3}+{A_T}^{1/3})[1+\beta_2{}^N Y_2{}^0(\theta)]$$
$$=R_V[1+\beta_2{}^N Y_2^0(\theta)]$$

to second order approximation. The $\beta_2{}^N$ value thus differs from the usually quoted $\beta_2{}^N(T)$ relative to the target (and not potential) deformation. We always took equal deformation values for the real and imaginary part of the potential. As for the Coulomb radius R_C, we always, unless stated otherwise, adopted

$$R_C(\theta)=1.2{A_T}^{1/3}[1+\beta_2{}^C Y_2{}^0(\theta)]\ , \qquad (4)$$

which according to Carter *et al.*[26] gives a better approximation of double folded Coulomb potential.

(iii) We limited our calculation to inelastic scattering towards the first excited state of each of the entrance channel nuclei, because it is usually located at an energy much lower than the following excited levels, a fact that enables it to absorb the greater part of the inelastic strength.

TABLE VI. Table of optical and deformation parameters used to calculate the fusion strength with a coupled-channels code (see text for more details). These parameters were taken from the quoted literature and are relevant to the system itself or to a mass-neighboring one. Asterisks refer to parameters taken from references marked also by asterisks.

System	V (MeV)	R_V (fm)	a_V (fm)	W (fm)	R_W (MeV)	a_W (fm)	$\beta_2{}^N(1)$	$\beta_2{}^C(1)$	$R_c(1)$ (fm)	$\beta_2{}^N(2)$	$\beta_2{}^C(2)$	$R_C(2)$ (fm)	Ref.
$^{24}Mg_1+{}^{12}C_2$	36	6.207	0.52	4.0	6.207	0.52	0.29	0.498	Eq. (4)	−0.283*	−0.283*	R_V	28,*:29
$^{28}Si_1+{}^{12}C_2$	41	6.392	0.52	4.2	6.392	0.52	−0.29	−0.466	Eq. (4)	−0.275*	−0.275*	R_V	28,*:29
$^{24}Mg+{}^{24}Mg$	100	6.980	0.49	7.0	7.269	0.26	0.245	0.498	Eq. (4)				30
$^{24}Mg_1+{}^{26}Mg_2$	100	7.075	0.49	7.0	7.367	0.26	0.245	0.498	Eq. (4)	0.169*	0.270*	Eq. (4)	30,*:31
$^{24}Mg_1+{}^{28}Si_2$[a]	100	7.165	0.49	7.0	7.459	0.26	0.29	0.498*	Eq. (4)	−0.138	−0.466*	Eq. (4)	30,*:28
$^{28}Si+{}^{28}Si$	20.5	8.077	0.45	2.5	7.652	0.26	−0.135	−0.135	R_V				30
$^{28}Si_1+{}^{29}Si_2$	20.5	8.124	0.45	2.5	7.697	0.26	−0.134	−0.466	Eq. (4)	0.152*	0.215**	Eq. (4)	30,*:32 **:33
$^{28}Si_1+{}^{30}Si_2$	20.5	8.171	0.45	2.5	7.740	0.26	−0.133	−0.466	Eq. (4)	0.130*	0.281*	Eq. (4)	30,*:34

[a]Exceptionally $\sigma_{\mathrm{in}}(2)$ was calculated with a different optical parametrization relevant to $^{28}Si+{}^{28}Si$.

(iv) The reaction cross section σ_{R_1} corresponds to the excitation of the most deformed of the two incident nuclei or of the one which has the lowest lying first inelastic state; the intermediate fusion strength is given by $\sigma_{F_1}=\sigma_{R_1}-\sigma_{\text{in}}(1)$, and the final $\sigma_{\text{CF}}=\sigma_{R_1}-\sigma_{\text{in}}(1)-\sigma_{\text{in}}(2)$ is comparable to our experimental fusion data.

Results

We present in Figs. 15–17 some of the theoretical fusion excitation functions compared to experiment, in order to illustrate the different kinds of agreement which can be obtained.

(a) In the case of $^{24}\text{Mg}+^{12}\text{C}$, theory and experiment compare rather well; the theoretical overestimate of σ_{CF} at low energy might be due to the slight experimental underestimation we pointed out in Sec. IV A 1. At energies higher than $E_{12_C}=40$, 42 MeV, it is more likely that other inelastic phenomena do occur, which contribute to lowering the theoretical fusion strength.

We have also reported in this figure one of the few available inelastic scattering ($^{24}\text{Mg}_{2^+}^{1.37\text{ MeV}}$) integrated excitation functions,[27] and one can see that our calculation gives a very good account of the mean absolute value of this inelastic strength, a fact that seems to confirm the accuracy of our approach.

(b) The agreement obtained for the $^{28}\text{Si}+^{29,30}\text{Si}$ is quite remarkable, as can be seen in Fig. 16. The $^{28}\text{Si}+^{28}\text{Si}$ system is very well reproduced up to $E_{\text{c.m.}}\simeq 35$ MeV. From this energy it might be possible that part of the lacking flux $\sigma_{\text{CF}}(\text{th})-\sigma_{\text{CF}}(\text{exp})$ is absorbed by mutual excitation of the first (1.78 MeV) level, a phenomenon that cannot be taken in account by the ECIS code.

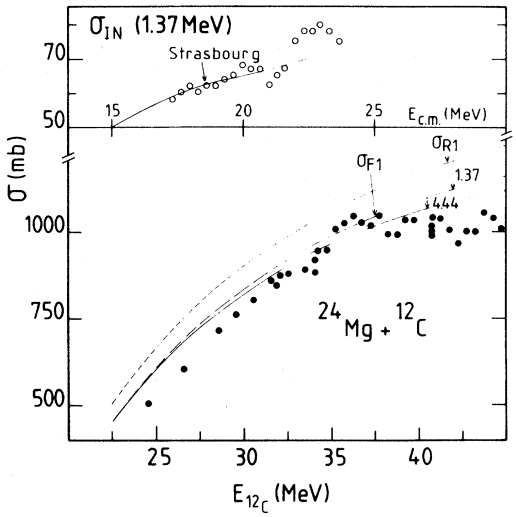

FIG. 15. Experimental fusion cross sections relative to $^{24}\text{Mg}+^{12}\text{C}$ compared to the theoretical predictions given by a coupled-channels calculation (full line), using parameters of Table VI (see text). The top inset compares experimental integrated inelastic (1.37 MeV) cross section (Ref. 27) to the predictions of the coupled-channels calculation.

(c) The two systems $^{24}\text{Mg}+^{24,26}\text{Mg}$ (Fig. 17) should be discussed in parallel. For $^{24}\text{Mg}+^{26}\text{Mg}$, we adopted an optical parametrization, coming from the analysis of angular distributions relative to $^{24}\text{Mg}+^{24}\text{Mg}$ elastic and inelastic scattering, and the agreement obtained with experimental data is very good. On the contrary, for $^{24}\text{Mg}+^{24}\text{Mg}$, the predicted $\sigma_{\text{CF}}(E)$ disagrees with the experimental points in the whole range of energy. We think that, at high energy, the mutual excitation of the 1.37 MeV level can account for the lacking cross section, but at low energy ($E_{\text{c.m.}}<28$, 29 MeV),

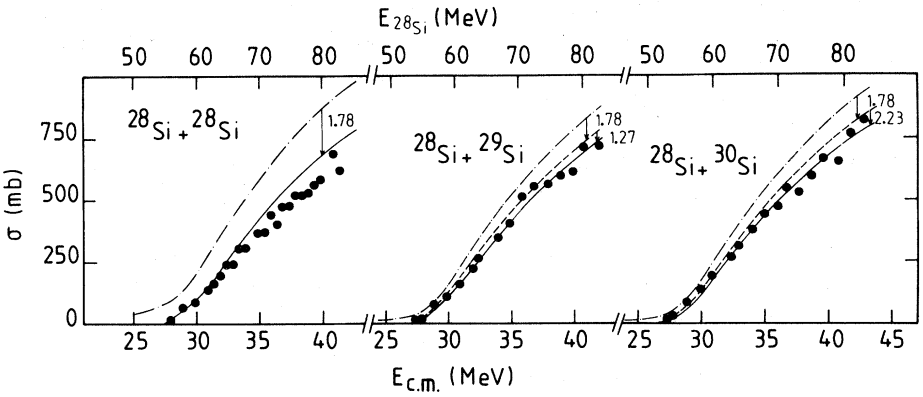

FIG. 16. Same as Fig. 15 for the $^{28}\text{Si}+^{28-30}\text{Si}$ systems.

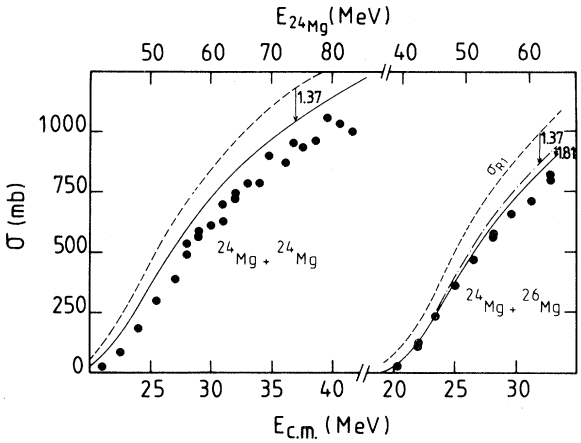

FIG. 17. Same as Fig. 15 for the $^{24}Mg+^{24,26}Mg$ systems.

the question remains to be answered as to what phenomenon could lower the fusion cross section by such a factor. Let us point out that this behavior of the low-energy part is peculiar whatever the analysis (see subsections 2 and 3).

(d) In the case of $^{28}Si+^{12}C$, for which no figure is presented, the agreement is good up to $E_{c.m.} \simeq 20$ MeV, but afterwards the theoretical fusion strength is quite overestimated (up to $\simeq 100$ mb). As for $^{28}Si+^{24}Mg$, the agreement is also quite satisfactory up to $E_{c.m.} \simeq 35$ MeV.

V. CONCLUSION

In this work we have studied the behavior of fusion cross sections, for several intermediate-mass systems, in an energy region dominated by the interaction barrier. Part of our motivation was to see if an appropriate choice of entrance channel nuclei (^{24}Mg, ^{28}Si, ^{12}C) could lead to oscillations of $\sigma_{CF}(E)$ similar to those observed in lighter mass systems $^{12}C+^{12}C$, ^{16}O and $^{16}O+^{16}O$.

In the range of energies we have studied, only the $^{24}Mg+^{12}C$ and $^{28}Si+^{28}Si$ systems seem to present slight oscillations in $\sigma_{CF}(E)$, but their amplitude ($< \pm 7\%$) is in no way comparable to those observed for lighter systems. No detectable structures were found for $^{28}Si+^{12}C$, $^{24}Mg+^{28}Si$, ^{24}Mg fusion excitation functions, although these systems were selected because of their entrance channels singularities.

The deexcitation of the compound nuclei formed by the various systems has also been studied, since an appropriate detection allowed us to identify the heavy residues. The comparison of experimental data to the theoretical predictions of the CASCADE code revealed no surprise apart from an unexplained high strength relative to the (CN-1 nucleon) residue of $^{28}Si+^{12}C$ fusion; we also observed a theoretical underestimation of the 2α decay mode, a feature that has already been observed for lighter nuclei at a similar excitation energy. The comparison of the experimental decay strengths relative to $^{28}Si+^{28-30}Si$ shows a very clear similarity of the decay patterns which are related only to E^*_{CN}, and neglect the details of the various nuclei involved in the deexcitation.

A comparison of $\sigma_{CF}(E)$ with systematic theoretical cross sections, such as the ones given by the Bass model, shows that one can reach a reasonable agreement with a macroscopic model. At the highest energies studied the influence of neutron excess on the absolute value of cross sections ($^{28}Si+^{28-30}Si$, $^{24}Mg+^{24,26}Mg$) does not exceed what is due to the change of radius of the target; the two light systems $^{14}N+^{12}C$ and $^{15}N+^{12}C$ thus seem to be the only ones to exhibit important differences of cross sections at the same energy. Nevertheless, a detailed comparison with the Bass model estimates points out clearly the shortcomings of such a macroscopic model; these limitations have lead us to attempt a more original approach to the fusion strength based on coupled-channels calculations, which try to take into account the specificity of entrance channel nuclei. We have thus reproduced in a very satisfactory fashion the absolute values and trends of $\sigma_{CF}(E)$ for nearly all the systems we studied. Nevertheless, it would be very helpful to dispose of integrated inelastic cross sections to confirm the validity of our approach ($^{24}Mg+^{12}C$, $^{24}Mg+^{24,26}Mg$, $^{28}Si+^{24}Mg$, $^{28-30}Si$), or help to establish why it fails ($^{28}Si+^{12}C$, low bombarding energy part relative to the $^{24}Mg+^{24}Mg$ system).

ACKNOWLEDGMENTS

We must thank particularly F. Saint-Laurent for his kind participation during the measurements. The help of H. Oeschler for the data analysis relative to $^{12}C_P+^{24}Mg_T$ is also gratefully acknowledged.

*Present address: Commissariat à l'Energie Atomique, 94190 Villeneuve-Saint-Georges, France.

[1]M. Conjeaud, S. Gary, S. Harar, and J. P. Wieleczko, Nucl. Phys. A309, 515 (1978).

[2]P. Sperr, T. H. Braid, Y. Eisen, D. G. Kovar, F. W. Prosser, and J. P. Schiffer, Phys. Rev. Lett. 37, 321 (1976).

[3]P. Sperr, S. Vigdor, Y. Eisen, W. Henning, D. G. Kovar, T. R. Ophel, and B. Zeidman, Phys. Rev. Lett. 36, 405 (1976).

[4]J. J. Kolata, R. C. Fuller, R. M. Freeman, F. Haas, B. Heusch, and A. Gallmann, Phys. Rev. C 16, 891 (1977).

[5]D. G. Kovar, in Proceedings of the IPCR Symposium on Macroscopic Features of Heavy Ion Collisions and Preequilibrium Process, Hakone, 1977, IPCR Cyclotron Report Suppl. 6, 1977.

[6]R. G. Stokstad, Y. Eisen, S. Kaplanis, D. Pelte, U. Smilansky, and I. Tserruya, Phys. Rev. Lett. 41, 465 (1977).

[7]R. G. Stokstad, W. Reisdorf, K. D. Hildenbrand, J. V. Kratz, G. Wirth, R. Lucas, and J. Poitou, Z. Phys. A 295, 269 (1980).

[8]W. Scobel, A. Mignerey, M. Blann, and H. H. Gutbrod, Phys. Rev. C 11, 1701 (1975).

[9]M. R. Clover, R. M. DeVries, V. Fulton, R. Ost, N. J. A. Rust, N. Anantamaran, J. L. C. Ford, and D. Shapira, in *Clustering Aspects of Nuclear Structure and Nuclear Reactions (Winnipeg, 1978),* Proceedings on the Third International Conference on Clustering Aspects of Nuclear Structure and Nuclear Reactions, edited by W. T. H. Van Oers and J. P. Svenne (AIP, New York, 1978).

[10]M. R. Clover, R. M. DeVries, R. Ost, N. J. A. Rust, R. N. Cherry, and H. E. Gove, Phys. Rev. Lett. 40, 1008 (1978).

[11]A. Gamp, W. Bohne, P. Braun-Munzinger, and C. K. Gelbke, Nucl. Instrum. Methods 120, 281 (1974).

[12]F. Pühlhofer, Nucl. Phys. A280, 267 (1977); and private communication.

[13]F. Saint-Laurent, thesis, Orsay, 1978 (unpublished).

[14]F. Saint-Laurent, M. Conjeaud, S. Harar, J. M. Loiseaux, J. Menet, and J. B. Viano, Nucl. Phys. A327, 517 (1979).

[15]F. Pühlhofer, W. F. W. Schneider, F. Busch, J. Barette, P. Braun-Munzinger, C. K. Gelbke, and H. Wegner, Phys. Rev. C 16, 1010 (1977).

[16]M. C. Mermaz, A. Greiner, E. Müller, B. T. Kim, M. Petrascu, M. Petrovici, and V. Simion, in the International Conference on the Resonant Behavior of Heavy Ion Systems, Aegean Sea, 1980 (unpublished).

[17]W. J. Jordan, J. V. Maher, and J. C. Peng, Phys. Lett. 87B, 38 (1979).

[18]H. Doubre, A. Lazzarini, K. T. Lesko, D. Leach, A. Seamster, and R. Van den Bosch, Washington Annual report, 1980 (unpublished), p. 113.

[19]S. B. Dicenzo, J. F. Petersen, and R. R. Betts, in contributed abstract to the Proceedings of the International Conference on Nuclear Physics, Berkeley, 1980, LBL Report No. LBL-11118, 1980.

[20]D. G. Kovar, D. F. Geesaman, T. H. Braid, Y. Eisen, W. Henning, T. R. Ophel, M. Paul, K. E. Rehm, S. J. Sanders, P. Sperr, J. P. Schiffer, S. L. Tabor, S. Vigdor, B. Zeidman, and F. W. Prosser, Phys. Rev. C 20, 1305 (1979).

[21]D. Horn and A. J. Ferguson, Phys. Rev. Lett. 41, 1529 (1978).

[22]M. Lozano and G. Madurga, Phys. Lett. 90B, 50 (1980).

[23]M. Lozano and G. Madurga (private communication).

[24]R. Bass, Phys. Rev. Lett. 39, 265 (1977).

[25]J. Raynal, Saclay Report DPh-T/71-48, 1971.

[26]J. Carter, R. G. Clarkson, V. Hnizdo, R. J. Keddy, D. W. Mingay, F. Osterfeld, and J. P. F. Sellschop, Nucl. Phys. A273, 523 (1976).

[27]R. M. Freeman, F. Haas, B. Heusch, and S. M. Lee, Phys. Rev. C 20, 569 (1979).

[28]J. S. Eck, D. O. Elliott, W. J. Thompson, and F. T. Baker, Phys. Rev. C 16, 1020 (1977).

[29]R. H. Bassel, G. R. Satchler, and R. M. Drisko, Nucl. Phys. 89, 419 (1966).

[30]H. Emling, R. Nowotny, D. Pelte, G. Schrieder, and W. Weidenmeier, Nucl. Phys. A239, 172 (1975).

[31]V. H. Rotberg and W. Mittig, Phys. Rev. C 22, 1574 (1980).

[32]E. Fabrici, S. Micheletti, M. Pignanelli, F. G. Resmini, R. de Leo, G. D'Erasmo, and A. Pantaleo, Phys. Rev. C 21, 844 (1980).

[33]D. Schwalm, E. K. Warburton, and J. W. Olness, Nucl. Phys. A293, 425 (1977).

[34]F. Todd Baker, A. Scott, E. E. Gross, D. C. Hensley, and D. L. Hillis, Nucl. Phys. A325, 525 (1979).

[35]R. G. Stokstad and E. E. Gross, Phys. Rev. C 23, 281 (1981).